Research Article | Vol. 25, No. 21 | 16 Oct 2017 | OPTICS EXPRESS 26221
Optics EXPRESS

Dynamically tunable plasmon induced absorption in graphene-assisted metallodielectric grating

TIAN ZHANG,[1] JIAN DAI,[1] YITANG DAI,[1] YUTING FAN,[1] XU HAN,[2] JIANQIANG LI,[1] FEIFEI YIN,[1] YUE ZHOU,[1] AND KUN XU[1,3,*]

[1]*State Key Laboratory of Information Photonics and Optical Communications, Beijing University of Posts and Telecommunications, Beijing 100876, China*
[2]*Wuhan National Laboratory for Optoelectronics, Huazhong University of Science and Technology, Wuhan 430074, China*
[3]*School of Science, Beijing University of Posts and Telecommunications, Beijing 100876, China*
**xukun@bupt.edu.cn*

Abstract: The dynamically tunable plasmon induced absorption (PIA) effect is demonstrated in a graphene-assisted metallodielectric grating structure. Two methods are employed to achieve the tunable PIA effect in the mid-infrared region: one is based on controlling the chemical potential of graphene by adjusting the gate voltage, the other is related to varying the refractive index of interlayer. Our calculated results reveal that high tunability in amplitude and bandwidth of the PIA effect can be achieved by using the above-mentioned methods. Compared with previous results, our scheme is much easier to fabricate and has significant applications in modulators, absorbers and sensors.

OCIS codes: (240.6680) Surface plasmons; (310.2790) Guided waves; (230.1950) Diffraction gratings; (050.6624) Subwavelength structures.

References and links

1. S. Zhang, D. A. Genov, Y. Wang, M. Liu, and X. Zhang, "Plasmon-induced transparency in metamaterials," Phys. Rev. Lett. **101**(4), 047401 (2008).
2. R. Taubert, M. Hentschel, J. Kästel, and H. W. Giessen, "Classical analog of electromagnetically induced absorption in plasmonics," in *Quantum Electronics and Laser Science Conference*, (Optical Society of America, 2012), QW1B. 1.
3. R. Taubert, M. Hentschel, and H. Giessen, "Plasmonic analog of electromagnetically induced absorption: simulations, experiments, and coupled oscillator analysis," J. Opt. Soc. Am. B **30**(12), 3123–3134 (2013).
4. P. Tassin, L. Zhang, R. Zhao, A. Jain, T. Koschny, and C. M. Soukoulis, "Electromagnetically induced transparency and absorption in metamaterials: the radiating two-oscillator model and its experimental confirmation," Phys. Rev. Lett. **109**(18), 187401 (2012).
5. J. He, P. Ding, J. Wang, C. Fan, and E. Liang, "Ultra-narrow band perfect absorbers based on plasmonic analog of electromagnetically induced absorption," Opt. Express **23**(5), 6083–6091 (2015).
6. H.-J. Li, L.-L. Wang, and X. Zhai, "Plasmonically induced absorption and transparency based on MIM waveguides with concentric nanorings," IEEE Photonics Technol. Lett. **28**(13), 1454–1457 (2016).
7. K. Wen, Y. Hu, L. Chen, J. Zhou, M. He, L. Lei, and Z. Meng, "Plasmonic-induced absorption and transparency based on a compact ring-groove joint MIM waveguide structure," IEEE Photonics J. **8**(5), 1–8 (2016).
8. M. Wen, L. Wang, X. Zhai, Q. Lin, and S. Xia, "Dynamically tunable plasmon-induced absorption in resonator-coupled graphene waveguide," Europhys. Lett. **116**(4), 44004 (2017).
9. X. Zhang, N. Xu, K. Qu, Z. Tian, R. Singh, J. Han, G. S. Agarwal, and W. Zhang, "Electromagnetically induced absorption in a three-resonator metasurface system," Sci. Rep. **5**, 10737 (2015).
10. Y. Li, B. An, S. Jiang, J. Gao, Y. Chen, and S. Pan, "Plasmonic induced triple-band absorber for sensor application," Opt. Express **23**(13), 17607–17612 (2015).
11. E. Sakat, G. Vincent, P. Ghenuche, N. Bardou, S. Collin, F. Pardo, J.-L. Pelouard, and R. Haïdar, "Guided mode resonance in subwavelength metallodielectric free-standing grating for bandpass filtering," Opt. Lett. **36**(16), 3054–3056 (2011).
12. E. Sakat, S. Héron, P. Bouchon, G. Vincent, F. Pardo, S. Collin, J.-L. Pelouard, and R. Haïdar, "Metal-dielectric bi-atomic structure for angular-tolerant spectral filtering," Opt. Lett. **38**(4), 425–427 (2013).
13. Y. Liang, W. Peng, R. Hu, and L. Xie, "Extraordinary optical properties in the subwavelength metallodielectric free-standing grating," Opt. Express **22**(16), 19484–19494 (2014).
14. T. Zentgraf, S. Zhang, R. F. Oulton, and X. Zhang, "Ultranarrow coupling-induced transparency bands in hybrid plasmonic systems," Phys. Rev. B **80**(19), 195415 (2009).

#302686 https://doi.org/10.1364/OE.25.026221
Journal © 2017 Received 21 Jul 2017; revised 20 Sep 2017; accepted 9 Oct 2017; published 13 Oct 2017

Optics EXPRESS

15. J. Zhang, W. Bai, L. Cai, Y. Xu, G. Song, and Q. Gan, "Observation of ultra-narrow band plasmon induced transparency based on large-area hybrid plasmon-waveguide systems," Appl. Phys. Lett. **99**(18), 181120 (2011).
16. W. Gao, J. Shu, C. Qiu, and Q. Xu, "Excitation of plasmonic waves in graphene by guided-mode resonances," ACS Nano **6**(9), 7806–7813 (2012).
17. T. Zhang, L. Chen, B. Wang, and X. Li, "Tunable broadband plasmonic field enhancement on a graphene surface using a normal-incidence plane wave at mid-infrared frequencies," Sci. Rep. **5**, 11195 (2015).
18. Y. Liang, W. Peng, R. Hu, and M. Lu, "Symmetry-reduced double layer metallic grating structure for dual-wavelength spectral filtering," Opt. Express **22**(10), 11633–11645 (2014).
19. Y. Liang, W. Peng, M. Lu, and S. Chu, "Narrow-band wavelength tunable filter based on asymmetric double layer metallic grating," Opt. Express **23**(11), 14434–14445 (2015).
20. Z. Chai, X. Hu, Y. Zhu, F. Zhang, H. Yang, and Q. Gong, "Low-power and ultrafast all-optical tunable plasmon-induced transparency in plasmonic nanostructures," Appl. Phys. Lett. **102**(20), 201119 (2013).
21. A. Vakil and N. Engheta, "Transformation optics using graphene," Science **332**(6035), 1291–1294 (2011).
22. T. Zhang, L. Chen, and X. Li, "Graphene-based tunable broadband hyperlens for far-field subdiffraction imaging at mid-infrared frequencies," Opt. Express **21**(18), 20888–20899 (2013).
23. X. Han, T. Wang, X. Li, B. Liu, Y. He, and J. Tang, "Ultrafast and low-power dynamically tunable plasmon-induced transparencies in compact aperture-coupled rectangular resonators," J. Lightwave Technol. **33**(14), 3083–3090 (2015).
24. Z. He, H. Li, S. Zhan, B. Li, Z. Chen, and H. Xu, "Tunable multi-switching in plasmonic waveguide with Kerr nonlinear resonator," Sci. Rep. **5**, 15837 (2015).
25. W. Albrecht, T.-S. Deng, B. Goris, M. A. van Huis, S. Bals, and A. van Blaaderen, "Single particle deformation and analysis of silica-coated gold nanorods before and after femtosecond laser pulse excitation," Nano Lett. **16**(3), 1818–1825 (2016).
26. G. Vincent, S. Collin, N. Bardou, J. L. Pelouard, and R. Haïdar, "Large-area dielectric and metallic freestanding gratings for midinfrared optical filtering applications," J. Vac. Sci. Technol. B **26**(6), 1852–1855 (2008).
27. A. Grigorenko, M. Polini, and K. Novoselov, "Graphene plasmonics," Nat. Photonics **6**(11), 749–758 (2012).
28. A. Christ, S. G. Tikhodeev, N. A. Gippius, J. Kuhl, and H. Giessen, "Waveguide-plasmon polaritons: strong coupling of photonic and electronic resonances in a metallic photonic crystal slab," Phys. Rev. Lett. **91**(18), 183901 (2003).
29. X. Han, T. Wang, X. Li, S. Xiao, and Y. Zhu, "Dynamically tunable plasmon induced transparency in a graphene-based nanoribbon waveguide coupled with graphene rectangular resonators structure on sapphire substrate," Opt. Express **23**(25), 31945–31955 (2015).
30. T. Zhang, X. Yin, L. Chen, and X. Li, "Ultra-compact polarization beam splitter utilizing a graphene-based asymmetrical directional coupler," Opt. Lett. **41**(2), 356–359 (2016).
31. H. J. Xu, W. B. Lu, W. Zhu, Z. G. Dong, and T. J. Cui, "Efficient manipulation of surface plasmon polariton waves in graphene," Appl. Phys. Lett. **100**(24), 243110 (2012).
32. I. T. Lin, C. Fan, and J. M. Liu, "Propagating and localized graphene surface plasmon polaritons on a grating structure," IEEE J. Sel. Top. Quantum Electron. **23**(1), 144–147 (2017).
33. C. H. Gan, "Analysis of surface plasmon excitation at terahertz frequencies with highly doped graphene sheets via attenuated total reflection," Appl. Phys. Lett. **101**(11), 111609 (2012).
34. H. Yan, X. Li, B. Chandra, G. Tulevski, Y. Wu, M. Freitag, W. Zhu, P. Avouris, and F. Xia, "Tunable infrared plasmonic devices using graphene/insulator stacks," Nat. Nanotechnol. **7**(5), 330–334 (2012).
35. C. Casiraghi, A. Hartschuh, E. Lidorikis, H. Qian, H. Harutyunyan, T. Gokus, K. S. Novoselov, and A. C. Ferrari, "Rayleigh imaging of graphene and graphene layers," Nano Lett. **7**(9), 2711–2717 (2007).
36. A. Yariv and P. Yeh, *Optical Waves in Crystals* (Wiley New York, 1984).
37. H. B. Liao, R. F. Xiao, J. S. Fu, H. Wang, K. S. Wong, and G. K. Wong, "Origin of third-order optical nonlinearity in Au:SiO 2 composite films on femtosecond and picosecond time scales," Opt. Lett. **23**(5), 388–390 (1998).
38. X. Piao, S. Yu, and N. Park, "Control of Fano asymmetry in plasmon induced transparency and its application to plasmonic waveguide modulator," Opt. Express **20**(17), 18994–18999 (2012).
39. C. Min, P. Wang, C. Chen, Y. Deng, Y. Lu, H. Ming, T. Ning, Y. Zhou, and G. Yang, "All-optical switching in subwavelength metallic grating structure containing nonlinear optical materials," Opt. Lett. **33**(8), 869–871 (2008).
40. X. Yang, X. Hu, Z. Chai, C. Lu, H. Yang, and Q. Gong, "Tunable ultracompact chip-integrated multichannel filter based on plasmon-induced transparencies," Appl. Phys. Lett. **104**(22), 221114 (2014).
41. Y. Zhu, X. Hu, Y. Fu, H. Yang, and Q. Gong, "Ultralow-power and ultrafast all-optical tunable plasmon-induced transparency in metamaterials at optical communication range," Sci. Rep. **3**, 2338 (2013).
42. S. Link, C. Burda, M. Mohamed, B. Nikoobakht, and M. A. El-Sayed, "Laser photothermal melting and fragmentation of gold nanorods: energy and laser pulse-width dependence," J. Phys. Chem. A **103**(9), 1165–1170 (1999).
43. J. Leuthold, W. Freude, J. M. Brosi, R. Baets, P. Dumon, I. Biaggio, M. L. Scimeca, F. Diederich, B. Frank, and C. Koos, "Silicon Organic Hybrid Technology—A Platform for Practical Nonlinear Optics," Proc. IEEE **97**(7), 1304–1316 (2009).
44. G. Xing, H. Guo, X. Zhang, T. C. Sum, and C. H. A. Huan, "The Physics of ultrafast saturable absorption in graphene," Opt. Express **18**(5), 4564–4573 (2010).

Optics EXPRESS

1. Introduction

Plasmon induced transparency (PIT) effect, which is a plasmonic analog to the quantum electromagnetic induced transparency, has attracted a great deal of attention due to abnormal dispersion and momentous applications [1]. Compared to the PIT effect, the plasmon induced absorption (PIA) effect also arises from the constructive interference of the bright and dark modes, leading to a sharp dip within a relatively broad transmittance peak [2]. It possesses abnormal dispersion, unique fast-light features, a narrow line-width accompanied with the enhanced absorbance, and practical applications including optical switching, fast light, optical modulator, sensor, absorber and so on [3–5]. Until now, in order to obtain the PIA effect, diversified plasmonic structures have been proposed, including plasmonic waveguide coupled with nanocavities (PWCN) [6–8] and metamaterials [2, 5, 9, 10]. However, limited by the microfabrication etching precision, these structures are relatively complicated to fabricate by current fabrication process. In addition, few studies have addressed the tunable PIA effect. Obviously, it is very valuable to design a structure, which is much easier to fabricate and could achieve the dynamically tunable PIA effect. In recent years, the researches on hybrid plasmonic mode coupling in subwavelength metal-dielectric nanostructures have attracted enormous attention due to its extraordinary optical properties [11–15]. Among various subwavelength plasmonic structures, the metallic grating coupled with dielectric waveguide layer (GCDWL) structures are of special interest for ultra-narrow bandwidth and relatively simple fabrication process [11, 12], offering a new way to obtain desired PIA effect. However, to our knowledge, few studies have realized the PIA effect based on the GCDWL structure.

It is noteworthy that, the excitation of surface plasmon polaritons (SPPs) on the surface of graphene with low propagation loss and high confinement can be observed in a plasmonic structure composed of monolayer graphene and a silicon diffractive grating [16, 17]. Thus, it is a promising method to excite the SPPs mode on graphene layer by employing the metal diffractive grating in the GCDWL structure, providing an efficient way to achieve the significant PIA effect. The past few years, tuning the operating window in the GCDWL has been realized by several approaches [18–20]. However, these methods primarily depend on altering the permittivity of high-index dielectric waveguide layer based on the Kerr effect or changing the geometrical parameters of the GCDWL structure. More importantly, the conductivity of graphene can be dynamically tuned by changing the chemical potential via chemical doping, electrostatic gating, and magnetic field [21, 22]. It would contribute to the realization of the PIA effect with dynamical tunability, which is of crucial importance for various actively optical devices, including optical modulator, switching and so on [23, 24].

Motivated by the above fundamental studies, in this article, a graphene-assisted metallodielectric grating (GMG) structure is proposed to realize the dynamically tunable PIA effect in the mid-infrared region. The constructive interference of the bright and dark modes induces the PIA effect in the transmission spectrum of the GMG structure, where the hybrid mode in the GCDWL structure acts as the bright mode, and the SPPs mode on graphene excited by the underneath metal grating acts as the dark mode. Our calculated results reveal that the amplitude and bandwidth of the PIA effect can be significantly tuned by varying the chemical potential of the graphene layer. As a comparison, the other two methods which have been reported for tuning the operating window [18–20] are also implemented in our research, namely, altering the thickness and the permittivity of the dielectric waveguide in the GMG structure. In addition, at oblique incidence, we also observe that the suppression of the absorption peak is accompanied with a higher reflection and a lower transmission by increasing the incident angles, showing potential applications in optical modulator, absorber, switching and so on.

2. Device design

The proposed GMG structure is exhibited in Fig. 1 schematically. Obviously, the structure is free-standing and it comprises a gold film periodically pierced by narrow slits and a thin SiN_x

Optics EXPRESS

waveguide layer. The thickness of the SiN_x film and the grating period are fixed to be d_s = 540 nm and Λ = 3800 nm, respectively. On consideration, we select the thickness of gold grating and the width of the gold and slit as d_{Au} = 70 nm, w_1 = 3585 nm and w_2 = 215 nm, respectively, and keep them fixed in the following simulations. The frequency-dependent permittivity of gold is described by well-known Drude model $\varepsilon_{Au}(\lambda) = 1-[(\lambda_p/\lambda + i\gamma)\lambda_p/\lambda]^{-1}$, where λ_p = 160 nm represents the plasma wavelength and γ = 0.0077 denotes the metal loss [11]. The monolayer graphene and grating are separated by a spacer layer with thickness d_i = 15 nm. For simplicity, the linear refractive index of the interlayer is assumed as n_i = 1.47 here. Certainly, silica and PMMA can be selected as the interlayer because they are colloidal which can reduce the deformation of the gold grating effectively [25]. Moreover, we will discuss the choice of the interlayer for the pump-tuning method in another section below.

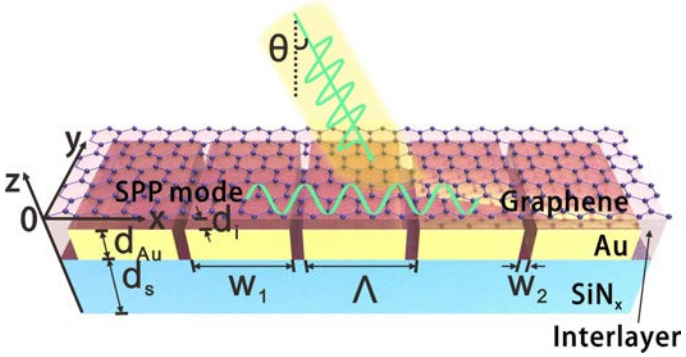

Fig. 1. Structure schematic of the proposed GMG structure.

It is rather remarkable that our proposed GMG structure can be fabricated by current nanofabrication technology. First of all, A 540-nm-thick SiN_x layer is deposited by plasma enhanced chemical vapor deposition (PECVD) on a 300-μm-thick silicon substrate, followed by a PECVD of the silica on the other side. Secondly, a 70-nm-thick gold grating structure is fabricated by using electron beam lithography (EBL) and liftoff process [11]. Thirdly, the gold grating is coated with interlayer on the top of the sample. Fourthly, a 3mm × 3 mm window is opened in the backside silica layer and the silicon substrate is etched in tetramethyl ammonium hydroxide solution, forming a free standing SiN_x film [11, 26]. Fifthly, graphene grown by Chemical Vapour Deposition (CVD) is transferred onto the surface of the interlayer. Finally, a gate voltage is applied between the monolayer graphene and the SiN_x waveguide layer to control the chemical potential of the graphene [16, 17, 22, 27].

3. Calculated results and discussions

First of all, in order to understand the PIA effect which would occur in our designed GMG structure, we study the optical response of the metallodielectric grating (MG) structure [Fig. 2(a)]. Here, the geometry parameters of the MG structure are set same as that of the above GMG structure. When TM-polarized plane wave normally incident onto the MG structure, the simulated transmission spectrum is presented as the blue solid line in Fig. 2(b). Here, the characteristic spectral responses are calculated using the finite-difference time-domain (FDTD) method (adopting commercial software Lumerical FDTD Solutions). In our simulations, the periodic boundary conditions are used in *x* direction, and the other boundaries employ the perfectly matched layer (PML) boundary conditions. Apparently, it can be observed that a transmission peak up to 73% emerges at the resonant wavelength λ = 4.53 μm. The reason for the occurrence of this abnormal transmission peak is related to the Fano resonance, which is attributed to the destructive interference between a wideband bright mode and a narrowband dark mode [11–13]. Here, the wideband bright mode in the MG structure relates to the zeroth diffraction order of grating, which can directly transmit through the gold grating; while the narrowband dark mode relates to the ± 1 diffraction orders trapping in the SiN_x dielectric layer [11, 28]. It is rather remarkable that the interlayer upon

Optics EXPRESS

the gold grating does not contribute to the abnormal transmission effect, because removing the interlayer from the MG structure only blue-shift the abnormal transmission peak as shown in the black dashed line. In order to clearly understand the mechanism for the generation of the transmission peak (λ = 4.53 μm) and dip (λ = 4.7 μm), we calculate the corresponding normalized magnetic field distributions and the simulation results are shown in Figs. 2(c) and 2(d), respectively. It is clearly shown in Fig. 2(c) that the guide mode resonance along the *x* direction is excited in the SiN_x dielectric film. However, the magnetic field intensity in the SiN_x dielectric layer at the transmission dip [Fig. 2(d)] is much weaker than that at the transmission peak [Fig. 1(c)], which means that the guided mode in the SiN_x dielectric waveguide layer is slightly excited at the transmission dip.

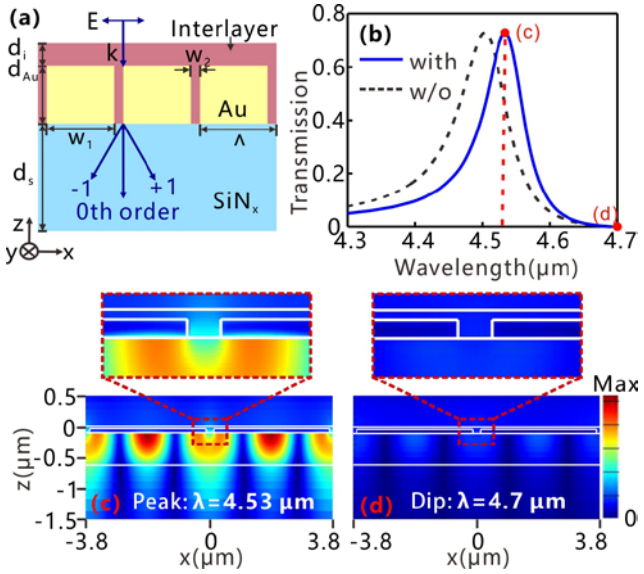

Fig. 2. (a) The schematic of the MG structure. (b) The simulated transmission spectrums when a TM-polarized light normally incident onto the MG structure with (blue solid line) and without (black dashed line) the interlayer upon the gold grating. Spatial magnetic field distributions for the MG structure with interlayer at λ = 4.53 μm (c) and λ = 4.7 μm (d).

Next, we come back to consider the characteristic spectrum response of the GMG structure [shown in Fig. 1]. In order to obtain the SPP modes on the GMG structure, we view one period of the GMG structure as two Fabry-perot cavities consisting of air-graphene-interlayer-S_iN_x (AGIS) model and air-graphene-interlayer-gold (AGIG) model. According to Maxwell equations of $\nabla \times \vec{E} = -j\omega\mu_0\vec{H}$ and $\nabla \times \vec{H} = j\omega\varepsilon_0\overline{\overline{\varepsilon}}_m\vec{E}$, the expression of electric and magnetic fields can be given as follows:

$$\nabla \times \vec{E} = -j\omega\mu_0\vec{H} \tag{1a}$$

$$\nabla \times \vec{H} = j\omega\varepsilon_0\overline{\overline{\varepsilon}}_m\vec{E} \tag{1b}$$

where ε_0 is the free space permittivity, μ_0 is the free space permeability, ω is the angular frequency, and $\overline{\overline{\varepsilon}}_m$ (m = 0, g, i, s) are the tensors of relative permittivities of air (m = 0), graphene (m = g), interlayer (m = i), and SiN_x (m = s), respectively. They all have the form:

$$\overline{\overline{\varepsilon}}_m = \begin{bmatrix} \varepsilon_{mx} & 0 & 0 \\ 0 & \varepsilon_{my} & 0 \\ 0 & 0 & \varepsilon_{mz} \end{bmatrix} \tag{2}$$

Optics EXPRESS

where ε_{mx}, ε_{my} and ε_{mz} are the corresponding relative permittivities at x-, y- and z-directions. For the designed GMG structure, the graphene is modeled as an anisotropic material whose in-plane permittivity is different from the out-of-plane one (2.5) [29, 30], its in-plane permittivity is described as ε_g. And three remaining materials are all isotropic. That is:

$$\varepsilon_{0x} = \varepsilon_{0y} = \varepsilon_{0z} = \varepsilon_0 \tag{3a}$$

$$\varepsilon_{gx} = \varepsilon_{gy} = \varepsilon_g, \varepsilon_{gz} = 2.5 \tag{3b}$$

$$\varepsilon_{ix} = \varepsilon_{iy} = \varepsilon_{iz} = \varepsilon_i \tag{3c}$$

$$\varepsilon_{sx} = \varepsilon_{sy} = \varepsilon_{sz} = \varepsilon_s \tag{3d}$$

For the TM modes supported on graphene (H_x, H_z, E_y = 0), we can obtain the following equations deduced from Eqs. (1) and (2):

$$H_y = \begin{cases} Ae^{j\beta x}e^{-k_s z}, & z < -d_g - d_i - d_{Au} \\ Be^{j\beta x}e^{k_i z} + Ce^{j\beta x}e^{-k_i z}, & -d_g - d_i - d_{Au} < z < -d_g \\ De^{j\beta x}e^{k_g z} + Ee^{j\beta x}e^{-k_g z}, & -d_g < z < 0 \\ Fe^{j\beta x}e^{k_0 z}, & z > 0 \end{cases} \tag{4}$$

$$E_z = \begin{cases} -A\dfrac{\beta}{\omega\varepsilon_0\varepsilon_{sz}}e^{j\beta x}e^{-k_s z}, & z < -d_g - d_i - d_{Au} \\ -B\dfrac{\beta}{\omega\varepsilon_0\varepsilon_{iz}}e^{j\beta x}e^{k_i z} - C\dfrac{\beta}{\omega\varepsilon_0\varepsilon_{iz}}e^{j\beta x}e^{-k_i z}, & -d_g - d_i - d_{Au} < z < -d_g \\ -D\dfrac{\beta}{\omega\varepsilon_0\varepsilon_{gz}}e^{j\beta x}e^{k_g z} - E\dfrac{\beta}{\omega\varepsilon_0\varepsilon_{gz}}e^{j\beta x}e^{-k_g z}, & -d_g < z < 0 \\ -F\dfrac{\beta}{\omega\varepsilon_0\varepsilon_{0z}}e^{j\beta x}e^{-k_0 z}, & z > 0 \end{cases} \tag{5}$$

where ε_{my}, $k_m = (\beta^2 - \varepsilon_{my}k_0^2)^{1/2}$ and d_m (m = 0, g, i, s) are the relative permittivities along y-axis, wavevectors and thicknesses of air (m = 0), graphene (m = g), interlayer (m = i), and SiN_x (m = s), respectively, and β is the propagation constant of the SPPs on AGIS models. Applying the continuous boundary conditions of H_y and E_x at three interfaces ($z = -d_g-d_i-d_{Au}$, $z = -d_g$, $z = 0$) and substituting the Eq. (3), we can obtain [31, 32]:

$$e^{-2k_i(d_i+d_{Au})} = \frac{1+\dfrac{\varepsilon_i k_s}{\varepsilon_s k_i}\cdot\left(1+\dfrac{\varepsilon_i k_g}{\varepsilon_g k_i}\right)\left(1+\dfrac{\varepsilon_g k_0}{\varepsilon_0 k_g}\right)+\left(1-\dfrac{\varepsilon_i k_g}{\varepsilon_g k_i}\right)\left(1-\dfrac{\varepsilon_g k_0}{\varepsilon_0 k_g}\right)e^{-2k_g d_g}}{1-\dfrac{\varepsilon_i k_s}{\varepsilon_s k_i}\left(1-\dfrac{\varepsilon_i k_g}{\varepsilon_g k_i}\right)\left(1+\dfrac{\varepsilon_g k_0}{\varepsilon_0 k_g}\right)+\left(1+\dfrac{\varepsilon_i k_g}{\varepsilon_g k_i}\right)\left(1-\dfrac{\varepsilon_g k_0}{\varepsilon_0 k_g}\right)e^{-2k_g d_g}} \tag{6}$$

Thus, using the similar derivation process, we can obtain the dispersion relation of the AGIG model:

$$1+\left(\frac{\varepsilon_0}{\varepsilon_i}-\frac{\beta'}{\omega\varepsilon_i}\frac{ne^2\mu_c}{\pi\hbar^2\omega}\right)\tanh\left(\beta' d_i\right) = 0 \tag{7}$$

where β' is the propagation constant of the SPPs on AGIG models. Here, the in-plane permittivity of graphene is described as $\varepsilon_g = 1 + i\sigma_g\eta_0/(k_0 d_g)$, where σ_g and η_0 (≈377 Ω) are the surface conductivity of graphene and impedance of air, respectively. It should be noted that

Optics EXPRESS

the increasing of the layer number of graphene sheets would weak the confinement of SPPs along graphene sheets [33], leading to a smaller phase-mismatching between the SPPs mode on graphene and wavevector in vacuum. Thus, in order to excite the SPPs mode on graphene more easily, we assume the layer number of graphene sheets as N = 3 in our design. Single layer of graphene is of thickness Δ = 0.34 nm, corresponding to the total thickness d_g = 1.02 nm and total conductivity $\sigma_g = N\sigma_{g,s}$, where $\sigma_{g,s}$ is the surface conductivity of single layer graphene [34, 35]. The $\sigma_{g,s}$ can be retrieved by the Kubo formula based on the dyadic Green's functions [16, 17, 22, 27]:

$$\sigma_{g,s} = i\frac{e^2 k_B T}{4\pi\hbar^2\left(\omega + i\tau^{-1}\right)}\left[\frac{\mu_c}{k_B T} + 2\ln\left(\exp\left(-\frac{\mu_c}{k_B T}\right)+1\right)\right] + i\frac{e^2}{4\pi\hbar}\ln\left[\frac{2|\mu_c| - \hbar\left(\omega + i\tau^{-1}\right)}{2|\mu_c| + \hbar\left(\omega + i\tau^{-1}\right)}\right] \tag{8}$$

here, k_B, T (= 300 K), $\hbar$,τ (= 0.5 ps), μ_c and e represent the represent the physical parameters of graphene (Boltzmann's constant, temperature, reduced Planck's constant, relaxation time, chemical potential, and electron charge), respectively.

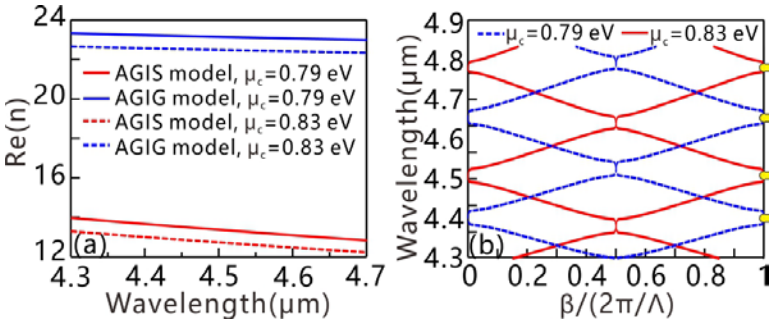

Fig. 3. (a) Calculated dispersion curves by employing Eqs. (6) and (7) for AGIS (two red lines) and AGIG (two blue lines) models with μ_c = 0.79 eV and μ_c = 0.83 eV, respectively. (b) Utilizing the calculated result in (a) and Eq. (9), the calculated band structure for the designed GMG structure with μ_c = 0.79 eV (blue dashed line) and μ_c = 0.83 eV (red solid line), respectively.

The dispersion relations of the SPPs represented by Eqs. (6) and (7) for different chemical potential are calculated as shown in Fig. 3(a). It can be found from the solid lines for μ_c = 0.79 eV that the gold under the graphene contributes to the enhancement of the field confinement of SPPs near the graphene layers. Furthermore, the chemical potential of graphene layers in the GMG structure could be tuned by the bias voltage applied on graphene based on the electric-field effect. We can find from Fig. 3(a) that tuning the chemical potential of graphene would significantly influence the dispersion for both AGIS and AGIG model, showing the potential in tuning the optical response of the GMG structure. With the acquirement of the dispersion of AGIS and AGIG model, we can obtain the band structure of the GMG structure by using the well-known secular equation [36]

$$\cos(\beta\Lambda) = \cos(k_1 w_1)\cos(k_2 w_2) - \frac{1}{2}\left(\frac{n_1}{n_2} + \frac{n_2}{n_1}\right)\sin(k_1 w_1)\sin(k_2 w_2) \tag{9}$$

where n_j and $k_j = n_j\omega/c$ (j = 1, 2) are the effective refractive index and wave vector of SPPs in the AGIS and AGIG model, respectively. The calculated band structure of the GMG is acquired by employing Eq. (9) as shown in Fig. 3(b). It should be noted that the plasmonic mode can be excited on the graphene layers of the GMG structure only when the grating period satisfies the phase-matching condition [16, 17, 37]

Optics EXPRESS

$$\mathrm{Re}(\beta) = k_0 \sin\theta + q\frac{2\pi}{\Lambda} \tag{10}$$

where q is the diffraction order, and θ is the incident angle. For the condition with normal incidence θ = 0°, Eq. (10) can be written as Re(β) = $2\pi q/\Lambda$. By employing this simplified equation at first diffraction order (q = 1), we can obtain the exciting wavelength of the SPPs in the GMG structure from 4.3 μm to 4.7 μm as the yellow dots shown in Fig. 3(b) [λ = 4.565 and 4.378 μm for μ_c = 0.83 eV, and λ = 4.658 and 4.454 μm for μ_c = 0.79 eV].

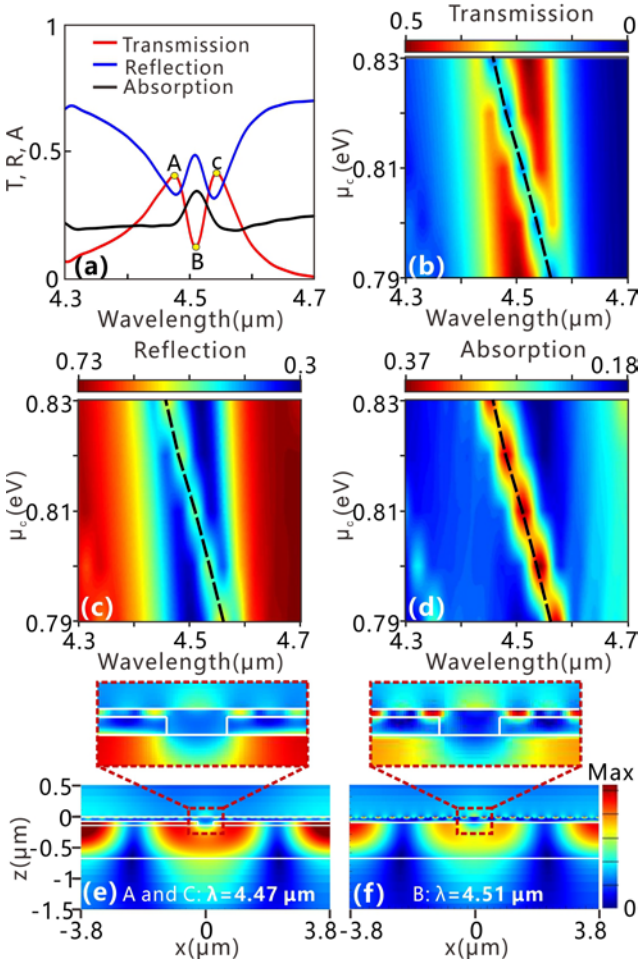

Fig. 4. (a) When normally incident electromagnetic wave onto the GMG structure, calculated transmission, reflection and absorption spectrums. (b-d) Evolutions of the transmission (b), reflection (c) and absorption (d) spectrum versus chemical potential of graphene and wavelength. (e, f) Distributions of the magnetic field corresponding to two transmission peaks and one transmission dip represented by A, C, and B points in (a).

When TM polarized light normally illuminates onto the GMG structure, the transmission, reflection and absorption spectrums are calculated by FDTD method for the graphene layers with μ_c = 0.81 eV, and the results are shown in Fig. 4(a). In our simulation, the mesh size inside graphene is kept as d_z = 0.17 nm (6 layers for the whole graphene sheets), which is small enough to ensure the numerical convergence. It is obvious that two transmission peaks which are indicated by point A and C emerge in the forbidden band and the central wavelengths of the peaks are 4.47 μm and 4.54 μm, respectively. It is noteworthy that one resonance dip is located between two peaks distinctly, which indicates that the PIA window

Optics EXPRESS

indeed appears in the transmission spectrum. In order to get more insight into the physics mechanism of the double transmission peaks and one resonance dip, the normalized magnetic field distribution of the resonance dip indicated by B point (at wavelength of 4.5 μm) is exhibited in Fig. 4(f). Compared with the normalized magnetic field distributions of the transmission peak at 4.47 μm [Fig. 4(e)], it's interesting to see that the strong SPPs modes are excited on the surface of the graphene, and the reason for this phenomenon is attributed to the diffraction by the gold grating. Herein, diffraction of the gold grating can bring about a relatively broad bandwidth for the zeroth diffracted order resonance, which forms the plasmonic bright mode. Then the wavevector mismatch between the plasmonic mode on the graphene layers and the incident light may be compensated by the gold grating. Namely, the plasmonic modes on the graphene which cannot be directly excited by the incident light form the "narrowband" plasmonic dark mode. It should be noted that the term "narrowband" is directed against the feature "wideband" of the bright mode. Due to the absorbing property of the graphene layers, the bandwidth of the dark mode is broadened inevitably. Actually, it can be found that the wavelength difference between the peak A and C in Fig. 4(a) is close to 100 nm. Obviously, the feature "narrowband" only means that the dark mode is narrowband relative to the bright mode. And the reduction of graphene's loss can result in the increase of the intrinsic quality factor of the dark mode. As shown in Fig. 4(f), it is the guided mode resonance excited on the graphene that suppresses the transmission peak shown in Fig. 2(b). Thus, we can attribute the appearance of the PIA effect to the destructive interference between guided mode resonance excited on the graphene and the zeroth diffracted order resonance in the GMG structure. It's worth noting that other dark mode (the ± 1 diffracted orders trapping in the SiN_x dielectric layer) also exists in the GMG structure, which leads to a transmission dip near to 4.70 μm. Thus, the GMG structure proposed here has one bright mode and two dark modes. In addition, the absorption peak (37%) located at 4.5 μm in Fig. 4(a) also confirms that the excitation of the plasmonic mode on the graphene. Obviously, the SPPs mode excited on the graphene can effectively improve the absorption of the GMG structure from 21% to 37%. What's more, as shown in Fig. 4(a), it is obvious that the pronounced PIT-like feature is demonstrated in the reflection spectrum. However, the difference between the reflection peak and dips is small, which is not conducive to the design of optical modulator and switching.

Moreover, electrical tuning of the PIA effect can be achieved by controlling the chemical potential of the graphene layers, and the evolutions of the transmission, reflection and absorption spectrums as a function of chemical potential and wavelength are calculated and shown in Figs. 4(b)-4(d), respectively. It is obvious that high tuning range can be achieved with a small change in the chemical potential of the graphene layers. We can observe that as the chemical potential increases, the transmission dip in Fig. 4(b), the reflection peak in Fig. 4(c) and the absorption peak in Fig. 4(d) are all blue-shifted, correspondingly. The black dotted lines in Figs. 4(b)-4(d), which are calculated by Eqs. (6)-(10), illustrate the change regulation of the resonant wavelength. One can see that the transmission peak of optical channel A is suppressed and that of optical channel B becomes prominent when the chemical potential increases from 0.79 eV to 0.83 eV in Fig. 4(b). In addition, the bandwidth of optical channel A drops and that of optical channel B is enlarged simultaneously. In Fig. 4(c), the increase of the chemical potential of graphene can lead to the transition of the reflection spectrum from PIT effect to Fano resonance. We attribute this phenomenon to the fact that the resonant wavelength of plasmonic mode on the graphene is sensitive to the change of chemical potential and hence the symmetry of the PIT effect is broken. What's more, in Fig. 4(d), the absorption peak is strongly dependent on the chemical potential of the graphene, enabling the flexible selectivity of operating spectral position. It provides a promising solution to obtain a tunable optical absorber in the mid-infrared region. Obviously, it is feasible to dynamically control the spectral positions of the optical channels by varying the gate voltage rather than altering the period and width of gold grating in the fabrication process.

Optics EXPRESS

Calculated transmission, reflection and absorption spectrum of the GMG structure for different thicknesses of the interlayer are exhibited in Figs. 5(a)-5(c), respectively. It is easy to expect that the PIA, PIT effect and the absorption peak are nonexistent when the thickness of the interlayer is thin. The reason for this is that the guided-mode resonance is not excited on the graphene. In the simulated results shown in Figs. 5(a)-5(c), as the thicknesses of the interlayer increases from 10 to 20 nm, the excitation wavelength of guided-mode resonance is varied and the PIT-like optical feature in (b) becomes asymmetry [38]. According to Eq. (9), we can attribute this phenomenon to that the resonant dips [D, E and F in Fig. 5(a)] caused by the guided-mode resonance on graphene are different order. It should be noticed that the transmittance of the dip at the central wavelength is not close to 0. The reason for this is associated with the loss of graphene layers. It is generally known that the loss of graphene is influenced by the graphene's momentum relaxation time τ. The larger the relaxation time τ is, the smaller the "loss" is. Here, the transmission spectrums for different relaxation times of the graphene layers are calculated and the corresponding results are shown in the inset of Fig. 5(a). When the relaxation times of graphene layers increase from 0.5 to 0.8 ps, the transmittance of the PIT effect at central wavelength changes from 0.17 to 0.10 simultaneously. As a result, the PIA effect can be optimized by controlling the relaxation time of graphene. Moreover, Figs. 5(d)-5(f) illustrate the simulated transmission, reflection and absorption spectrums of the GMG structure for different thicknesses of the SiN_x dielectric layer, respectively. It is seen that the transmission peak of the optical channel has an overall red-shift as the thicknesses of the SiN_x dielectric layer increases. The reason for this phenomenon can be explained by the dispersion equations of the GCDWL structure supported by ref [13]. Besides, it is rather remarkable that the excitation wavelength of the guided-mode resonance is independent of the increase of the SiN_x dielectric layer. Thus, the absorption peaks shown in Fig. 5(f) are stable when the thickness of the SiN_x waveguide layer increases from 540 nm to 600 nm.

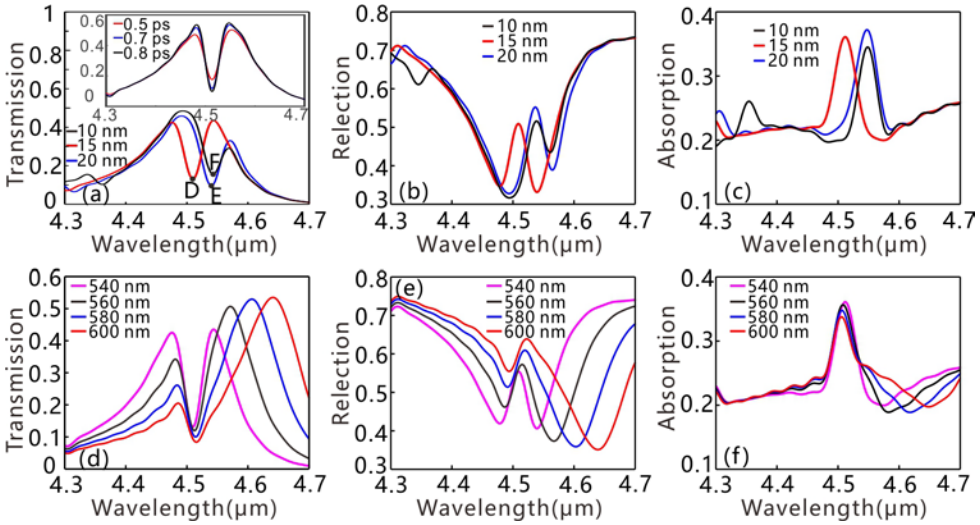

Fig. 5. Calculated transmission, reflection and absorption spectrums of the GMG structure for different thickness of the interlayer (a-c) and the SiN_x dielectric layer (d-f). The inset in (a) denotes the transmission spectrums for different relaxation times of graphene.

Next let us proceed to consider the nonlinear response of the GMG structure based on the Kerr effect. It's worth noting that other nonlinear responses are not taken into consideration here, such as third harmonic generation and two photon absorption effect [39]. According to Eqs. (6)-(10), the resonant wavelength of the plasmonic mode on the graphene depends on the chemical potential and the refractive index of the material upon the gold grating. As a result, we can control the resonant wavelength of the guided mode resonance on the graphene by changing the chemical potential or the dielectric constant of interlayer. Actually, the

Optics EXPRESS

interlayer between the graphene and gold grating can be replaced by the PMMA. Then, the dynamically tunable PIA effect can be achieved based on the thermo-optic effect, i.e., the refractive index of the PMMA coated on the gold grating changes with the temperature [40]. However, the response time of the thermally tuning method has been demonstrated several microseconds, which limits its extensive application [41]. In order to obtain the ultrafast tunability, the optical Kerr effect has been proposed to achieve the response time at the order of picosecond. However, it is not a simple issue for the GMG structure in the mid-infrared region, because many factors should be taken into consideration, including the deformation of gold grating by pump light, the selection of the Kerr material, the influence of the pump light on the interlayer and graphene, and the damage threshold of the graphene layers. Here, those factors are analyzed as follows: (1) As we known that gold grating can be deformed by thermal heating. It has been demonstrated that less pulse intensity is needed to deform the gold particles when using fs-pulses compared to ns pulses [42]. In addition, the deformation behavior can be affected by coatings surrounding gold nanorods [42] And the characteristic heat dissipation times of 2000 ps and 500 ps are estimated roughly for gold nanorobs and silica-coated gold nanorobs, respectively [25]. Obviously, in order to reduce the deformation of the gold grating, the duration of the pump light should be on the order of ps or ns. (2) The interlayer between the gold grating and graphene should be selected carefully to reduce the deformation of the gold grating. Although the Au:SiO_2 composite film has large third-order nonlinear susceptibility, it is not a suitable material due to its non-colloidal. Silica and PMMA are colloidal and can reduce the deformation of the gold grating effectively, but the third-order nonlinear susceptibilities are so small that giant pump intensity is required. The polymer composed of organic materials may be a reasonable alternative because it has large third-order nonlinear susceptibility and fast response time [43]. More importantly, the polymer should be colloidal and can be made mesoporous to reduce the deformation of the gold grating. (3) It should be noticed that the aggregation and enhancement of field in the interlayer and graphene can be obtained because the SPPs modes are excited on the graphene when TM polarized light normally illuminates on the GMG structure. There is no doubt that the aggregation and enhancement of field can affect the properties of the graphene and interlayer. It should be noted that, the electric field of the TM-polarized incident light is perpendicular to the nanowire of the grating (along x-axis), while the electric field of the TE-polarized incident light is parallel to the nanowire of the grating (along y-axis). Due to the different continuous boundary condition, TM-polarized incident light can excite the resonant SPPs modes on the grating, while the TE-polarized incident light can't. As a result, the pump light should be TE polarized to reduce the effect of the pump light on the graphene and interlayer. (4) The damage of graphene caused by fs-pulse or continuous wave laser also should be taken into account. It has been demonstrated that the damage threshold of graphene for femtosecond pulse laser and continuous wave laser is about 2.7 TW/cm^2 and 1 MW/cm^2, respectively [39]. The molecular lasers support the range of the pump intensity 0~10 MW/cm^2 for graphene layer [44]. The laser pulse with duration of fs is not suitable for our GMG structure, while ps or ns laser pulse may be appropriate choice. Here, for simplicity, the interlayer is assumed as Au:SiO_2 due to its giant Kerr coefficient ($\chi^{(3)} = 1.7 \times 10^{-7}$ esu) and ultra-fast response time [27,31]. And the wavelength of pump light and the chemical potential of graphene are taken to be 4 μm and 0.81 eV, respectively.

Figure 6(a) shows the simulated transmission, reflection and absorption spectrum of the GMG structure with different pump intensities (0 and 4.7 MW/cm^2). It is obvious that the tunable feature of the operating window can be obtained by increasing the intensity of the pump light. The resonant wavelength of the guide-mode resonance on the graphene is red-shift as the pump intensity increases from 0 to 4.7 MW/cm^2. It is attributed to the fact that the guided mode resonance excited on the graphene layers is sensitive to the refractive index of the interlayer. In addition, the evolutions of the transmission, reflection and absorption spectrums versus the refractive index of the Au:SiO_2 interlayer and wavelength are shown in Figs. 6(b)-6(d), respectively. It's important to note that the dashed lines in Figs. 6(b)-6(d) are theoretically resonant wavelengths corresponding to the guided mode resonance based on

Optics EXPRESS

Eqs. (6)-(10). As show in Fig. 6(b), it is interesting to notice that the optical channel on the left becomes more prominent and the optical channel on the right is gradually suppressed as the pump intensity increases. As shown in Fig. 6(c), the reflectance located at 4.5 μm is reduced from 0.5 to 0.35 when the pump intensity increases from 0 to 9.5 MW/cm^2, and the symmetry of the PIT effect is broken. In addition, as shown in Fig. 6(d), the increase of the pump intensity leads to the red-shift of the absorption peak and has a slight impact on the bandwidth of the peak. It can also be found that the theoretically calculated results are in good agreement with the simulated results shown in Figs. 6(b)-6(d). In order to calculate the switching time of our proposed GMG structure, a square pump light with intensity of 4.5 MW/cm^2 and duration time of 1.0 ps illuminates on the GMG structure. The simulated results based on the FDTD method are exhibited in Fig. 7(a). From the simulated results, the ultrafast switching times 0.36 ps can be achieved for switching up and down of the signal light. Here, it should be noted that the response time of the interlayer is not taken into consideration. The reason for this is that the final switching time is dependent on the response time of interlayer when the response time of interlayer is larger than 0.36 ps [39]. In addition, the deformation of the gold grating caused by laser pulse is also not taken into consideration [25]. Obviously, the switching time of our proposed GMG structure is at the picosecond level, which has some potential applications in ultrafast modulator and switching.

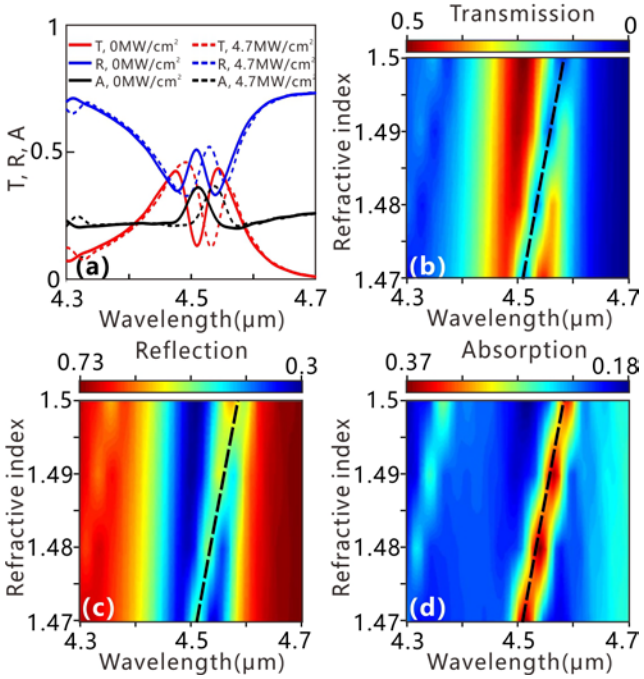

Fig. 6. (a) Calculated transmission, reflection and absorption spectrum of the GMG structure for different pump intensities under the condition of normal incidence. Evolution of the transmission (b), reflection (c) and absorption (d) spectrums versus the refractive index of the interlayer and wavelength.

Finally, we also investigate the influence of oblique incident light on the transmission, reflection and absorption spectrum. In order to avoid the influence of electric tuning method and pump light tuning method, the chemical potential of the graphene layers and the pump intensity are fixed as 0.81 eV and 0 MW/cm^2, respectively. In our simulations, the incident angle range is from 0° to 25° with a step of 5° and the Bloch boundary is employed in x direction. Figures 7(b)-7(d) show the simulated transmission, reflection and absorption spectrums of the GMG structure with different incident angle. It can be found that the increase of the incident angles not only results in the decrease of the transmission of the optical channels but also leads to the enhancement of the reflectance. In addition, the

Optics EXPRESS

suppression of the absorption peak can be observed in Fig. 7(d) as the increase of the incident angles. It means that the guide mode resonance excited on graphene layers becomes more difficult due to the increase of the incident angles. In summary at oblique incidence, we observe that the suppression of the absorption peak is accompanied with the higher reflection and the lower transmission. Certainly, it paves a new way towards the realization of dynamically tunable filter and absorber in the mid-infrared region based on our proposed GMG structure.

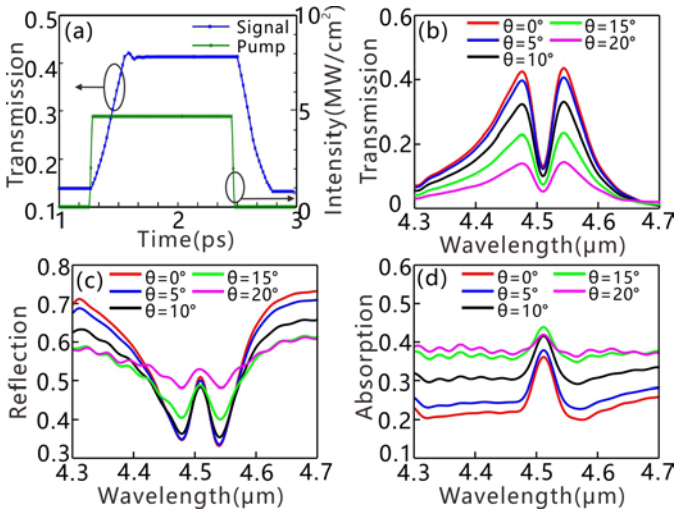

Fig. 7. (a) Transmittance of the dip at central wavelength of the PIA effect (blue line), and the green line denotes the intensity of a square pump pulse. (b-d) Calculated transmission, reflection and absorption spectrums of the GMG structure for different incident angles.

4. Conclusions

In conclusion, in this article, the dynamically tunable PIA effect is proposed and investigated in the GMG structure containing nonlinear Kerr medium. Our calculated results reveal that the amplitude and bandwidth of the PIA effect can be tuned by controlling the chemical potential of the graphene or altering the refractive index of the interlayer based on the Kerr effect. Moreover, it can be observed that the suppression of the absorption peak is accompanied with the higher reflection and the lower transmission by increasing the incident angle. Compared with previous results, our proposed GMG scheme is much easier to fabricate and the PIT effect has important applications in filters, modulators, absorbers and sensors in the mid-infrared region.

Funding

National Natural Science Foundation of China (Grant No. 61625104 and No. 61431003); China Postdoctoral Science Foundation (Grant No. 2017M610826); and National Key Research and Development program (Grant No. 2016YFA0301300).